Self-similar transport processes in a two-dimensional realization of multiscale magnetic field turbulence

Francesco Chiaravalloti
Dipartimento di Fisica, Università della Calabria, I-87036 Arcavacata di Rende, Italy

Alexander V. Milovanov*
Department of Physics, University of Tromsø, 9037 Tromsø, Norway
**Permanent address:*
Department of Space Plasma Physics, Space Research Institute,
84/32 Profsoyuznaya street, 117997 Moscow, Russia

Gaetano Zimbardo
Dipartimento di Fisica, Università della Calabria, I-87036 Arcavacata di Rende, Italy
Istituto Nazionale di Fisica della Materia, Unità di Cosenza, I-87036 Arcavacata di Rende, Italy

(February 2, 2008)

We present the results of a numerical investigation of charged-particle transport across a synthesized magnetic configuration composed of a constant homogeneous background field and a multiscale perturbation component simulating an effect of turbulence on the microscopic particle dynamics. Our main goal is to analyze the dispersion of ideal test particles faced to diverse conditions in the turbulent domain. Depending on the amplitude of the background field and the input test particle velocity, we observe distinct transport regimes ranging from subdiffusion of guiding centers in the limit of Hamiltonian dynamics to random walks on a percolating fractal array and further to nearly diffusive behavior of the mean-square particle displacement versus time. In all cases, we find complex microscopic structure of the particle motion revealing long-time rests and trapping phenomena, sporadically interrupted by the phases of active cross-field propagation reminiscent of Levy-walk statistics. These complex features persist even when the particle dispersion is diffusive. An interpretation of the results obtained is proposed in connection with the fractional kinetics paradigm extending the microscopic properties of transport far beyond the conventional picture of a Brownian random motion. A calculation of the transport exponent for random walks on a fractal lattice is advocated from topological arguments. An intriguing indication of the topological approach is a gap in the transport exponent separating Hamiltonian-like and fractal random walk-like dynamics, supported through the simulation.

I. INTRODUCTION

Anomalous transport phenomena in complex nonlinear dynamical systems can often be associated with the effect of turbulence on the microscopic particle kinetics. The multiscale interaction of nonlinear relaxation processes and self-organization mechanisms operating in turbulent media customarily results in a transition to a nonequilibrium (quasi)stationary state [1] dominated by long-range correlations in space and time [2]. In statistically homogeneous, isotropic systems, turbulent correlations at the (quasi)stationary state support self-similar transport regimes that are far beyond the conventional Gaussian diffusion. As a rule, such regimes explicitly involve the impacts of memory, intermittency, and nonlocality; examples are Levy-type processes [3–6] and fractal time random walks (FTRW's) [3,7,8], dating back to Mandelbrot and Van Ness fractional Brownian motion [9,10].

Levy processes incorporate bursty dynamics with almost instant multiscale jumps often referred to as "flights" [4]. The defining feature of Levy flights is a heavy tailed power-law jump length distribution leading to infinite second moments of the corresponding probability density. The problem of infinite moments may be avoided by replacing Levy flights with Levy walks through a spatiotemporal coupling posing inertia restrictions over the bursty events [11,12]. Levy walks provide suitable probabilistic model of superdiffusive transport [13] corresponding to faster-than-linear growth of the mean-square particle displacement versus time. In contrast to Levy flights, FTRW's are continuous random walk processes without identifiable jumps. Fractal time random walk statistics relies on a power-law distribution of waiting times between consequent steps of the motion [14]. FTRW's account for long-time particle rests in the turbulent medium and customarily result in slower-than-linear evolution of the tracer dispersion. A comprehension of the essential role played by FTRW and Levy statistics in the microscopic description of turbulence has led to a formulation of the fractional − "strange" − kinetics [15] reviewed in Refs. [16,17].

Near a (quasi)stationary state, the competition between fractal time and Levy walk regimes produces a self-similar trajectory with the variance which grows with time raised to a power between 0 and 2:

$$\left\langle \mathbf{r}^2(t)\right\rangle \sim 2\mathcal{D}t^{\mu}, \quad 0 \leq \mu \leq 2. \tag{1}$$

The quantity $\mathcal{D}$ in Eq. (1) has the sense of a generalized transport coefficient and is measured in units cm^2 s$^{-\mu}$. One distinguishes between subdiffusive ($\mu < 1$) and superdiffusive ($\mu > 1$) processes: The former are dominated by long-time rests, the latter, by "active" migration regimes such as Levy walks. The property of self-similarity appears in fractal structure of the trajectories over a broad range of spatial scales. The key parameter describing the topology of the particle track in the real space is the fractal dimension of the motion, $d_w \geq 1$ [18]. The value of d_w is related to the transport exponent μ in Eq. (1) via

$$\mu = 2/d_w, \quad d_w \geq 1. \tag{2}$$

Equation (2) holds both FTRW's and flights [16]. The transport regimes included in Eqs. (1) and (2) range from ballistic motion ($d_w = 1, \mu = 2$) to the confinement ($d_w = \infty, \mu = 0$). Diffusive processes correspond to $d_w = 2$ and $\mu = 1$. A realization of a trajectory having $d_w = 2$ is provided by the conventional Brownian random walk model [10] showing uncorrelated behavior on all time and spatial scales [16]. Note that the Brownian random motion on a plane covers densely everywhere the ambient two-dimensional space as time $t \to \infty$ [19]. In case of subdiffusion ($\mu < 1$), the trajectory covers the plane with excess density when compared to the random Brownian counterpart, meaning $d_w > 2$ in Eq. (2). The phenomenon is generally agreed to be due to multiscale memory effects which make the tracer return more often to the points already visited to time t. In contrast to subdiffusion, superdiffusive regimes ($\mu > 1$) suppress the returns, enabling "fast" tracks with the "low" dimension $d_w < 2$. An inherent drive for superdiffusion is often associated with spatiotemporal nonlocality [16], though its detailed comprehension is far from being complete [14].

In many cases, the subdiffusive ($\mu < 1$) behavior in Eq. (1) is supported by a self-organized concentration of turbulent transport processes on low-dimensional (fractal) arrays such as percolating lattices. [The term "percolating" is synonymous with "infinite connected," meaning a structure which stretches to arbitrary long (macroscopic) scales. In what follows, "connected" is understood in a somewhat restrictive sense "path-connected:" An arbitrary point found on a path-connected fractal set can propagate to another one along a continuous trajectory which lies everywhere on this set. The property of path-connectedness makes it possible to consider the fractal distribution as a *single* topological object.] Given a self-similar percolating fractal lattice with the Hausdorff dimension $d_f \geq 1$, one finds the mean-square displacement of the walker after time t to be [18]

$$\left\langle \mathbf{r}^2(t)\right\rangle \sim 2\mathcal{D}t^{2/(2+\theta)}. \tag{3}$$

The dispersion in Eq. (3) corresponds to the exponent $\mu = 2/(2+\theta)$ and the fractal dimension of the motion $d_w = 2+\theta$. The quantity θ is the index of connectivity of the fractal, which simultaneously appears in the probability to return to the starting point $p(t) \propto t^{-d_f/(2+\theta)}$ [20]. The index of connectivity describes intrinsic topological features of fractal objects [21] and observes remarkable invariance properties [22]. For path-connected fractal distributions, the value of $\theta \geq 0$ (as opposed to disconnected fractals having $\theta < 0$) [22]. In the limit of Euclidean (nonfractal) geometry, the index of connectivity $\theta \to 0$, leading to the conventional, Einstein relation $\left\langle \mathbf{r}^2(t)\right\rangle \sim 2\mathcal{D}t$ for the particle diffusion. Together with the Hausdorff dimension d_f, the index of connectivity

θ defines the so-called spectral (or fracton) dimension $d_s = 2d_f/(2+\theta) = 2d_f/d_w = \mu d_f$ [23]. The value of d_s determines the effective (fractional) number of degrees of freedom on a fractal geometry [24]. This fractional number is manifest in the scaling $p(t) \propto t^{-d_s/2}$, associated with the return probability $p(t)$ in a fractional "Euclidean" space enabling d_s "orthogonal" directions [22]. In view of $\theta \geq 0$, the value of the spectral dimension cannot exceed its Hausdorff counterpart as soon as the property of path-connectedness applies, $d_s \leq d_f$.

Physical realizations of strange transport processes (both subdiffusive and superdiffusive) encompass fluid [25] and electrostatic drift-wave turbulence [26,27], chaotic flows generated by multipoint vortices [28], self-avoiding random walks [29], disordered solid materials [30], astrophysical [31] and laboratory [32] plasma, including highly intermittent, self-similar regimes measured in the edge and scrape-off layer region of fusion devices [33]. In cosmic electrodynamics, unconventional statistical properties of transport bridging to the strange kinetics paradigm have been speculated for the solar photosphere [34], the Earth's dayside magnetopause [35,36], and the Earth's distant magnetotail [37,38].

In this paper, we analyze self-similar transport processes in a synthesized magnetic configuration composed of a constant homogeneous background field and a multiscale perturbation component simulating a marginal impact of turbulence on the behavior of test-particles. The physics included in the consideration below ranges from laboratory (fusion) realizations to typical conditions in space plasmas, specific to charged particle (ion) dynamics in turbulent magnetotail-like current sheets. Our study includes both numerical and theoretical counterparts. The details of the numerical magnetic field model along with the microscopic equations of motion are given in Sec. II. The basic transport regimes *a priori* speculated for the turbulent system concerned are addressed in Sec. III. Numerical simulation results for the particles faced to diverse conditions in the turbulent domain are presented in Sec. IV. We end with a summary in Sec. V.

II. MAGNETIC FIELD MODEL

Setting (x, y, z) to be Cartesian coordinates in a three-dimensional Euclidean space, we define the magnetic field configuration through $B_x = 0$, $B_y = 0$, and $B_z = B$, where

$$B \equiv B_0 + \delta B(\mathbf{r}), \quad \mathbf{r} \equiv (x, y, 0), \tag{4}$$

B_0 is a constant homogeneous background field, $\delta B(\mathbf{r})$ is a magnetostatic perturbation generated across the horizontal (xy) plane, and $\mathbf{B} = (0, 0, B)$ is the magnetic field vector looking everywhere in the direction normal to the plane, z. The existence of a zero-frequency, magnetostatic perturbation mode in a magnetized plasma was shown in Ref. [39]. This mode is reminiscent of the zero-frequency electrostatic convective-cell (vortex) mode [40] in two-dimensional plasma. In particular, the two modes share scaling properties of the cross-field transport coefficient above the classical collisional limit [39]. The behavior of extremely low-frequency perturbation modes in an unmagnetized plasma have been discussed by Ginzburg and Ruhadze [41]. The perturbation component in Eq. (4) is assumed in the form

$$\delta B(\mathbf{r}) = \sum_{\mathbf{k}} \delta B_{\mathbf{k}} \exp[i\mathbf{k}\cdot\mathbf{r} + i\varphi_{\mathbf{k}}], \tag{5}$$

where $\delta B_{\mathbf{k}}$ is the Fourier amplitude of the magnetostatic mode with wave vector $\mathbf{k} = (k_x, k_y, 0)$, and $\{\varphi_{\mathbf{k}}\}$ are random phases posing $-$ in the limit of statistical description $-$ the reflection symmetry $\delta B(\mathbf{r}) \leftrightarrow -\delta B(\mathbf{r})$. This mirrors the inherent parity properties of the multiscale magnetic field turbulence *in situ* measured in the Earth's magnetotail current sheet [42]. Owing to the reflection symmetry, the separatrix $B = B_0$ corresponding to the zero-set of the perturbation component $\delta B(\mathbf{r}) = 0$ contains a path-connected percolating subset [21] enabling field-line and magnetized charged-particle transport at the macroscopic scales [43]. The amplitudes $\delta B_{\mathbf{k}}$ introduced in the Fourier expansion in Eq. (4) are further defined through an algebraic function

$$\delta B_{\mathbf{k}} = \frac{2\pi A/L}{(k^2L^2 + 1)^{(\alpha+1)/4}}, \tag{6}$$

where $k = |\mathbf{k}|$ is the absolute value of the wave vector $\mathbf{k}$, L is the side of the square, double periodic simulation box, A is the normalization constant, and α is the slope of the Fourier power-law energy density spectrum, $P(k) \sim k^{-\alpha}$. Equations (5) and (6) define the so-called *fractional Brownian surfaces* [10], synthesized fractal objects incorporating generic features of percolation in irregular media [43]. [Here we ignore nonlinear effects like mode coupling and build-up of correlations which may destroy the wave-like features in Eq. (5). The role of nonlinearity has recently been emphasized in Refs. [27] and [44] in connection with the formation of coherent vortical structures in low-β plasmas, dominating the transport on individual flux-surfaces. In this study, we focus on the impact of fractal behavior on the microscopic particle dynamics, already present in the generic realization in Eqs. (5) and (6).]

In the numerical model, the components k_x and k_y are settled on the grid $k_x = 2\pi n_x/L$ and $k_y = 2\pi n_y/L$, with integer valued n_x and n_y; these satisfy $n_{\min}^2 \leq n_x^2 + n_y^2 \leq n_{\max}^2$. The $\mathbf{k}$ space is thereby a circular corona stretching from $k_{\min} = 2\pi n_{\min}/L$ to $k_{\max} = 2\pi n_{\max}/L$. For the runs presented below, $n_{\min} = 4$ and $n_{\max} = 80$. Accordingly, the turbulence wavelengths $\lambda = 2\pi/k$ range from $\lambda_{\min} = L/80$ to $\lambda_{\max} = L/4$. The shortest wavelength $\lambda_{\min}$ determines the finest scale of the inhomogeneities present, $a \sim \lambda_{\min}$. The longest wavelength $\lambda_{\max}$, in its turn, simulates the macroscopic turbulence correlation length, $\xi \sim \lambda_{\max}$. The ratio $\xi/a \sim 20$. This mimics the properties of the turbulence in the Earth's stretched and thinned magnetotail near a marginal (quasi)stationary state [38]. The number of independent Fourier modes in Eq. (5) is, by order of magnitude, $N \sim \pi(n_{\max}^2 - n_{\min}^2)/2 \sim 10^4$. A zero cut $\delta B(\mathbf{r}) = 0$ of the fractional Brownian surface in Eq. (5) is illustrated in Fig. 1.

The equation of motion for a particle of mass m and charge q, migrating across the magnetic field $\mathbf{B}$, reads

$$m\frac{d\mathbf{v}}{dt} = q\frac{\mathbf{v}\times\mathbf{B}}{c}, \tag{7}$$

where $\mathbf{v} = d\mathbf{r}/dt = (dx/dt, dy/dt, 0)$ is the velocity at point $\mathbf{r} = (x, y, 0)$ at time t. Denote $\rho \sim vmc/qB$ to be the particle Larmor radius in the magnetic field $\mathbf{B}$. (Here $v = |\mathbf{v}|$ is the absolute value of the velocity vector $\mathbf{v}$.) Let us further introduce dimensionless parameters $\ell \sim \rho/a$ and $b \sim \delta B/B_0$. The effective cross-field transport regime may be sensitive to ℓ and b, as we now proceed to show.

III. BASIC TRANSPORT REGIMES

A. Hamiltonian limit

Assume first $\ell \to +0$ and $b \ll 1$, meaning magnetized particles everywhere in the (xy) plane. As is well known [45], the dynamics of magnetized particles is adiabatic, enabling one to rely on a guiding center − drift − approximation of the long-time ($t \gg mc/qB_0$) particle motion. The guiding center drift velocity is given by [45]

$$\mathbf{u} = \frac{mc}{2q}\frac{v^2}{B_0}\frac{\mathbf{B}\times\nabla B}{B_0^2}, \tag{8}$$

leading to a system of Hamiltonian equations

$$\frac{dx}{dt} = \frac{\partial\Phi(x,y)}{\partial y}, \quad \frac{dy}{dt} = -\frac{\partial\Phi(x,y)}{\partial x}. \tag{9}$$

Here, $\Phi(x,y) = -(v^2/2B_0\Omega)\delta B(x,y)$ is time independent − stationary − Hamiltonian, and $\Omega \sim qB_0/mc$ is a characteristic particle gyrofrequency. The Hamiltonian $\Phi(x,y)$ is considered as the zero frequency limit ($\omega \to 0$) of a time varying, single frequency ($\propto e^{i\omega t}$) Hamiltonian $\Phi(x,y,t)$. Starting from the periodic Hamiltonian $\Phi(x,y,t)$ and turning the perturbation frequency to zero, $\omega \to 0$, one may demonstrate [19] that the main contribution to the cross-field transport comes from a thin layer surrounding the separatrix $B = B_0$, where the particle excursion periods along percolating isoenergetic contours resonate with the basic period of the field, $2\pi/\omega \to \infty$.

In many ways, the Hamiltonian dynamics in Eqs. (8) and (9) resembles the convection of a magnetized plasma by $\mathbf{E}\times\mathbf{B}$ drifts caused by zero-frequency electrostatic vortex modes across the externally applied confining magnetic field [40]. The ubiquitous zero frequency − static − limit $\omega \to 0$ extremizes the case of "strong" turbulence [46], conventionally described by the so-called Kubo number $\mathcal{Q} \sim u/\omega a \gg 1$, where $u = |\mathbf{u}|$ is the absolute value of the vector $\mathbf{u}$, and a/u is a typical migration time in the field. For $\mathcal{Q} \gg 1$, the large-scale behavior of the turbulent transport coefficient in Eq. (1) can be summarized by the power-law dependence [47]

$$\mathcal{D} \sim \frac{1}{2}a^2\omega^{2/d_w}\mathcal{Q}^{d_w/(2d_w-1)}, \tag{10}$$

where the fractal dimension $d_w \geq 1$ stands for the topology of the transport process in the real space. The factor ω^{2/d_w} behind a^2 accommodates the strange ($\propto t^{2/d_w}$) evolution of the variance $\langle \mathbf{r}^2(t)\rangle$ versus time t. In case of a diffusion ($d_w = 2$), the coefficient in Eq. (10) scales with $\mathcal{Q}$ as $\mathcal{Q}^{2/3}$. This contrasts the widely known Bohm scaling $\mathcal{D} \propto \mathcal{Q}^1$, which is traditionally affiliated with charged-particle diffusion in low-frequency wave fields, since the pioneering works in Refs. [39] and [40]. The deviation from the Bohm scaling mirrors the role of percolation properties in the guiding center picture of the cross-field particle transport [48].

As the perturbation frequency vanishes, $\omega \to 0$, the Kubo number in Eq. (10) diverges as an inverse, $\mathcal{Q} \to \infty$. The transport coefficient $\mathcal{D} \propto \omega^{2/d_w}\mathcal{Q}^{d_w/(2d_w-1)}$ then goes to zero if the fractal dimension of the motion satisfies $2/d_w > d_w/(2d_w - 1)$, yielding $1 \leq d_w < 2 + \sqrt{2}$. For $d_w \to 2+\sqrt{2} \approx 3.41$ [to be associated with the stationary Hamiltonian $\Phi(x,y)$ in Eq. (9)], the value of $\mathcal{D}$ saturates at

$$\mathcal{D} \sim a^{\sqrt{2}}u^{2-\sqrt{2}}/2 \tag{11}$$

and does not depend on ω. The corresponding transport law $\langle \mathbf{r}^2(t)\rangle \propto t^{\mu}$ is a *subdiffusion* with the exponent

$$\mu = 2 - \sqrt{2} \approx 0.58 \quad (t \to \infty). \tag{12}$$

The subdiffusive regime in Eq. (12) is dominated by long-time particle rests near the points of equilibrium, defined by $\partial\Phi/\partial x = 0$ and $\partial\Phi/\partial y = 0$. This behavior is asymptotic: $t \to \infty$. In view of Eq. (12), the coefficient in Eq. (11) observes anomalous scaling with the magnetic perturbation $b \ll 1$, i.e., $\mathcal{D} \propto b^{2-\sqrt{2}}$.

It is instructive to emphasize that the parameter $\mu = 2 - \sqrt{2}$ is the exact lower bound on the transport exponent for stochastic Hamiltonian systems with $1\frac{1}{2}$ degrees of freedom [47]. This lower bound is determined by the extremely long particle rests near the points of equilibrium, where the guiding center drift velocity vanishes. The prevalence of such long rests in the zero frequency limit suppresses the effect of topology of the separatrix on the cross-field transport rate. This appears in the fact that the value $\mu = 2 - \sqrt{2}$ does not depent on the details of the geometry of the array $B = B_0$, nor on the way the separatrix is folded in the ambient space. Such details come into play as soon as the magnetized (adiabatic) behavior is relaxed.

B. Random walks on a fractal array

Near the points of equilibrium, the Hamiltonian approximation in Eq. (9) is invalidated already for very small but finite values of the particle Larmor radius, $\ell \sim \rho/a$. Nonadiabatic effects are more pronounced in magnetic configurations with larger perturbation component, $b \sim \delta B/B_0$. The limitation $b \ll 1$ assumed in Eqs. (8) and (9) may now be loosen to $b \lesssim \mathcal{O}$, where $\mathcal{O}$ is a constant of the order of 1. Even if slight ($\ell \ll 1$), nonadiabaticity is important as it revives the particles attempting to rest at equilibrium. The phenomenon helps the charge carriers to keep up their mobility near the points of occasionally small magnetic gradients $\nabla B \to 0$. The cross-field particle migration is naturally enhanced in this case, implying $\mu \gtrsim 0.58$ in Eq. (1).

The inclusion of slight nonadiabaticity allows the particles to pass more readily through the points of equilibrium and thereby wander along the separatrix $B = B_0$ in an almost casual way. A suitable approach to the problem could be found within a class of random walk models [18] associated with the percolative geomety of the set $B = B_0$ [21].

In the case of an isotropic, random-phased perturbation such as the fractional Brownian surface in Eqs. (5) and (6), the separatrix $B = B_0$ forms a percolating array which observes, in addition to the path-connectedness, *fractal* properties in the range of scales between $a \sim \lambda_{\min}$ and $\xi \sim \lambda_{\max}$ (see Refs. [10] and [49]). Here, ξ has the sense of the (upper) fractal correlation length which is known to diverge at criticality, $\xi \to \infty$ [18]. For "physical" fractals, the value of ξ is of course finite ($\xi < \infty$), though far longer than a. The finiteness of ξ poses an upper bound where the fractal geometry of percolation crosses over to a statistically homogeneous distribution, $d_s \to d_f \to 2$.

In two ambient dimensions, the percolation along the separatrix is critical, meaning a threshold at the level $B = B_0$. Crossing the threshold one changes the domain which contains the paths to infinity [43]. The formation of critical percolating fractal structures has recently been conjectured as a generic property of the (quasi)stationary states in complex nonlinear dynamical systems far from thermal equilibrium [22].

The criticality character supports *universal* behavior of the percolation transition, manifest in a variety of intriguing properties such as independence of the type of the percolation problem and of the microscopic details of the lattice [43]. In what follows, we are interested in the universality of the spectral dimension d_s [23], first conjectured by Alexander and Orbach [50] and later addressed in an improved form by Milovanov [51] who introduced the notion of the *percolation constant* $\mathcal{C}$, a topological parameter incorporating the features of connectedness of fractal distributions. The percolation constant is defined as the smaller (between the two possible) root to the identity [51]

$$\mathcal{C}\frac{\pi^{\mathcal{C}/2}}{\Gamma(\mathcal{C}/2+1)} = \pi, \tag{13}$$

where the symbol Γ denotes the Euler gamma function. The value of $\mathcal{C}$, a transcendental parameter approximately equal to $1.327\ldots$, determines the least fractional number of degrees of freedom, enabling a particle to reach the point at infinity through a random walk process on a self-similar fractal geometry. A topological approach to the phenomenon of percolation leading to the identity in Eq. (13) is discussed in some detail in Ref. [22]. In terms of the percolation constant, the universality of the spectral dimension at the threshold is quantified by [51]

$$d_s \equiv 2d_f/(2+\theta) = \mathcal{C} \approx 1.327. \tag{14}$$

Once the number of degrees of freedom is known from Eq. (14), an evaluation of the exponent $\mu = 2/(2+\theta) = \mathcal{C}/d_f$ in Eq. (3) is reduced to a calculation of the Hausdorff dimension d_f of the lattice on which the transport process concentrates. For critical percolation on two-dimensional fractal arrays, the value of d_f lies within [52]

$$\mathcal{C} \leq d_f \leq \mathcal{S} \equiv \ln 8/\ln 3 = 1.89\ldots < 2, \tag{15}$$

where $\mathcal{S} \equiv \ln 8/\ln 3$ is the Hausdorff dimension of the square Sierpinski carpet [53], a celebrated topological object providing the universal embedding for paths on a plane [54]. Inequality (15) derives as a condition which brings together the property of path-connectedness and the threshold character, manifest in the fact that both $\mathcal{C}$ and $\mathcal{S}$ pose the restrictions on the Hausdorff dimension d_f. In view of $\mu = \mathcal{C}/d_f$ we have, at the critical range,

$$\mu_{\min} \leq \mu \leq 1, \tag{16}$$

$$\mu_{\min} = \mathcal{C}/\mathcal{S} \approx 0.70. \tag{17}$$

Note a gap $\Delta\mu \approx 0.12$ between $\mu_{\min} = \mathcal{C}/\mathcal{S} \approx 0.70$ and the Hamiltonian bound $\mu = 2 - \sqrt{2} \approx 0.58$ in Eq. (12). Owing to the gap, a transition from Hamiltonian dynamics to random walks on a fractal pattern may have an abrupt character, when a slight increase in the particle Larmor radius ℓ results in an almost sudden growth (from ≈ 0.58 up to at least 0.70) of the transport exponent μ. This makes the Hamiltonian regime in Eq. (12) appreciably sensible to the particle Larmor radius ℓ assumed in the simulation.

The exact value of the Hausdorff dimension d_f, specific to the topology of fractional Brownian surfaces, has been calculated in Ref. [21] from the shape of fractal isoenergetic contours in vicinity of the separatrix $B = B_0$:

$$d_f = 2\mathcal{C} - 1 \approx 1.65. \tag{18}$$

The Hausdorff dimension in Eq. (18) falls well inside the range defined by inequality (15). Relation (18) corresponds to the exponent of the Fourier energy density spectrum obeying $1 \leq \alpha \leq 7 - 4\mathcal{C} \approx 1.69$ [21]. The latter guarantees enough energy at the small scales, validating self-similar behavior of the microscopic kinetic process. Combining Eqs. (3), (14) and (18), one arrives at

$$\mu = \mathcal{C}/(2\mathcal{C} - 1) \approx 0.80. \tag{19}$$

The ensuing cross-field particle transport is a *subdiffusion*, $\langle \mathbf{r}^2(t) \rangle \propto t^{0.80}$. This is enhanced when compared to the subdiffusive behavior $\langle \mathbf{r}^2(t) \rangle \propto t^{0.58}$ in the limit of Hamiltonian dynamics quantified by Eqs. (8) and (9). The fractal dimension of the motion equals $d_w = 2/\mu = 2(2\mathcal{C} - 1)/\mathcal{C} \approx 2.49$ and is in fact lower than in the adiabatic case ($d_w = 2 + \sqrt{2} \approx 3.41$). A derivation of the turbulent transport coefficient $\mathcal{D}$ for the particles having small but finite Larmor radius $\ell \ll 1$ involves the issue of the branching dimension [19] and is intricate somewhat [35]. Here we note that $\mathcal{D}$ may not reveal a single scaling behavior, contrary to the Hamiltonian coefficient in Eqs. (10) and (11).

A subdiffusion consistent with the exponent in Eq. (19) has earlier been proposed for ions migrating across the turbulent magnetotail current sheet [38]. The estimate in Eq. (19) applies to the "anomalous" time scales $a^{2+\theta} \lesssim t \lesssim \xi^{2+\theta}$ for which the particles walk on the fractal. For longer times $t \gtrsim \xi^{2+\theta}$, the particles cover distances generally exceeding the fractal correlation length, ξ. This implies a transition to a random walk process on an Euclidean (nonfractal) geometry. Hence

$$\mu \to 1 \tag{20}$$

for $t \gtrsim \xi^{2+\theta}$. Consequently, the asymptotic ($t \to \infty$) behavior of the cross-field transport process in the slightly nonadiabatic case ($\ell \ll 1$, $b \lesssim \mathcal{O}$) should be *diffusive*. The corresponding particle diffusion coefficient is of the order of

$$\mathcal{D} \sim au/2. \tag{21}$$

The occurrence of the asymptotic ($t \to \infty$) diffusive regime already in the slightly nonadiabatic realization is in contrast to the magnetized particle dynamics relying on the Hamiltonian Eqs. (9). The latter is *subdiffusive* (with the exponent $\mu \approx 0.58$) on *all* time scales $t \gg 1/\Omega$, up to $t \to \infty$. Note that the diffusion cross-over time scale for random walks on a percolating fractal array diverges as $\xi^{2+\theta}$ for $\xi \to \infty$.

C. Strong nonadiabaticity

In the limit of strong ($\ell \gtrsim 1$) nonadiabaticity, the cross-field transport processes occupy wide stochastic domains, whose measure is comparable with that of the ambient Euclidean plane itself. The microscopic particle dynamics thereby evolves into random walks in two dimensions ($d_s \to d_f \to 2$), meaning *diffusive* behavior $\mu \to 1$ on the time scales $t \gg a/v$. The cross-field diffusion coefficient can be evaluated as [cf. Eq. (21)]

$$\mathcal{D} \sim av\ell/2. \tag{22}$$

Remark that the condition $\ell \gtrsim 1$ is always satisfied near the zero-set $\delta B(\mathbf{r}) = 0$ for vanishing background component, $B_0 \to 0$. The perturbation parameter diverges in this case, $b \to \infty$, signifying a decaying role of the percolation properties.

IV. NUMERICAL RESULTS

In this section, we present a selection of numerical runs which illustrate the basic transport regimes operating in the magnetic configuration in Eqs. (4)−(6). Magnetic field models with both nonvanishing and zero background component are investigated. All lengths are normalized to the side of the simulation box, L, and all times, to the inverse of the particle gyrofrequency, Ω. The running value of Ω refers to the local magnetic field B which may appreciably deviate from B_0. The particle velocity v is measured in units ΩL, with typical values ranging − for different realizations − from 2×10^{-4} to 5×10^{-4}. For each run, 5000 particles are injected in a random manner throughout the simulation box, $L \times L$. Initial velocity vectors $\mathbf{v}$ are randomly directed. The equation of motion (7) is solved numerically by means of a fifth-order Runge-Kutta integrator with adaptive step; the maximum time step is 10^{-2}. Depending on the strength of the background field B_0 and the exact value of the injection velocity v, the total integration time varies from 3×10^6 to 1×10^7. The accuracy of the computation is checked by various methods, including conservation energy verification at the end of the run, showing relative errors of less than 10^{-4}. The evaluation of the exponent μ is based on running fits with a time window $\Delta t \sim 10^6$, which is made gradually move along t.

A. Zero background component

A nearly diffusive regime is readily recovered for the zero background component $B_0 = 0$ (i.e., for the infinite perturbation parameter $b = \infty$). The details of the simulation are as follows. The particles are injected at random with the velocities $v = 5 \times 10^{-4}$. The integration is performed up to 3×10^6, enabling a rich statistics of tracking data. The value of the transport exponent computed over the whole set of the trajectories is found to be $\mu \approx 0.96 \pm 0.05$. This value incorporates the particles trapped on closed isoenergetic contours far from the separatrix, $B = B_0$. Simultaneously, the dispersion of those particles initialized in close vicinity of the zero-set $\delta B(\mathbf{r}) = 0$ and propagating to longest distances across the field is not distinguished from a diffusion-type process. Sample trajectories of such particles bringing a basic contribution in the cross-field transport are illustrated in Figs. 2 and 3. We draw attention to the very complex microscopic structure of the particle motion, revealing a chaotic alternation of long-time rest and sporadic transient periods, manifest in the highly irregular, intermittent way the trajectory is marked by the tracer. In this connection, the diffusion appears to be an intricate balance between the time intervals when the particles stay in traps, and the "green-light" regimes − reminiscent of Levy walk statistics − when the charge carriers actively migrate across the medium. This intriguing picture challenges the conventional Brownian random motion paradigm customarily associated with diffusion. We interpret this unusual behavior as a "strange diffusion" [22] deriving from a parity between rests and walks, the two competing counterparts of the dynamics underlying the transport at the microscopic scales.

B. Finite background component

We turn next to a situation with a finite background field B_0. To support the effect of the particle Larmor radius, we set $b \sim 2$ in the simulation below. This choice is a suitable compromise between the opposite extremes of $b \ll 1$ and $b = \infty$.

1. Random walks on a fractal array

As in the regime with zero background component, we set the injection velocity v to 5×10^{-4}. Accordingly, the integration covers time scales up to 3×10^6 and repeats the details of the run specified in subsection **A.** The particle dispersion versus time is plotted in Fig. 4, solid line. The fit yields $\mu \approx 0.84 \pm 0.05$. This value is clearly subdiffusive and complies with the exponent in Eq. (19). Consequently, we consider the estimate $\mu \approx 0.84 \pm 0.05$ as an evidence for a concentration of the cross-field transport on a percolating fractal array owing to the departure of B_0 from the zero limit.

To help judge the result obtained, we launch another run with all the same integration and test particle parameters, but with a filter in the injection scheme. As the filter is applied, the particles found "too far" from the percolation level $B = B_0$ are discarded. Thus, we only integrate along the trajectories that start in a band $B_0 \pm \Delta B$, with ΔB a fraction of B_0. We could thereby increase the portion of particles staying close to the percolation level and appreciably speed up the computation. The behavior of the particle dispersion for this run is shown in Fig. 4, dashed line. While larger distances are achieved, the exponent μ remains practically unchanged, $\mu \approx 0.86 \pm 0.05$. This observation proves that the transport, as a matter of fact, is mostly due to the particles migrating in close vicinity of the percolation level.

A realization of the percolation-associated particle trajectory in the presence of the background component is developed in Fig. 5. The tracer features a tendency toward adiabatic dynamics, manifest in the periods of a drift-like migration along the separatrix. Near the saddles of the zero-set $\delta B(\mathbf{r}) = 0$ (see Fig. 1), the drift-like regimes are interrupted by almost unmagnetized, meandering motion in a close-to-separatrix layer owing to the effect of finite Larmor radius. The observation of meandering is important as it supports the chance for casuality enabling to consider the cross-field transport in connection with random walk processes on percolative fractal geometry [18]. At the microscopic scales, the meandering motion bears signatures reminiscent of the intermittent dynamics found for $B_0 = 0$ (see Figs. 2 and 3). The drift, in its turn, exhibits inhomogeneous behavior with alternating phases of fast and slow progress. These competing phases of fast and slow migration acquire the role of the walk-and-rest statistics as the adiabatic limit is approached. We emphasize that the "walks" are inherently present in the motion, even though the ensuing transport appears to be subdiffusive. In this regard, the parity between walks and rests previously speculated for the strange diffusion is now shifted toward rests.

2. Back to diffusion

With increasing velocity v, the mean-square displacement of the tracer tends to a linear (diffusive) form starting from longer integration times. For shorter times, the dispersion may still be subdiffusive. For instance, turning v from 5×10^{-4} to 1×10^{-3}, we locate the transport exponent within $\mu \approx 0.95 \pm 0.05$ for the long integration time 1×10^7. As the integration time is reduced to 3×10^6, the fractal random walk-like dispersion $\mu \approx 0.84 \pm 0.05$ is recovered. Runs with larger velocities reveal nearly diffusive behavior already for the short times 3×10^6. These results demonstrate the effect of the finite fractal correlation length, ξ, posed by the basic periodicity of the simulation box. We emphasize that the periodic extension of the simulation box assumed in the simulation truncates the percolative fractal geometry of the field beyond $\xi \sim \lambda_{\max}$.

3. Hamiltonian limit

To approach the adiabatic regime in Eq. (9), we turn the injection velocity v to 2×10^{-4}. Simultaneously, we maintain the background component B_0 at the level corresponding to $b \sim 2$ in order to achieve a clearer comparison with the previous runs. A longer integration time 1×10^7 matching the proposed decrease in v is settled.

The particle dispersion as a function of time is summarized in Fig. 6.

As the velocity is set to 2×10^{-4}, a pronounced subdiffusive behavior is observed through the integration period. The fit yields $\mu \approx 0.67 \pm 0.05$, which is appreciably smaller than the values allowed for a random walk process on a fractal geometry [see Eqs. (17) and (19)]. The estimate of $\mu \approx 0.67 \pm 0.05$ is reminiscent of the exponent $\mu \approx 0.58$ in Eq. (12), corresponding to the limit of Hamiltonian dynamics. Some deviation between the numerical result $\mu \approx 0.67 \pm 0.05$ and the extreme of $\mu \approx 0.58$ could be due to the excessively large magnetic perturbation parameter, $b \sim 2$. This deviation may further be shown to decrease with increasing background field, B_0.

Turning, gradually, the injection velocity v from 5×10^{-4} to 2×10^{-4}, we find an unstable transitional behavior when the exponent μ fluctuates between Hamiltonian-like and fractal random walk-like values. This poses an uncertainity in μ for some intermediate values of v. To the major extent, the uncertainities are bypassed as v gets sufficiently close to 2×10^{-4}. We associate the observed unstable regimes with the existence of the gap deriving from Eqs. (12) and (17). On the contrary, no specific unstable domain is found for v varying between 5×10^{-4} and 1×10^{-3}, showing a continuous turnover to the diffusive transport.

A sample trajectory corresponding to the "cold" particles with velocities $v = 2 \times 10^{-4}$ is plotted in Fig. 7. The motion is drift-like everywhere along the isoenergetic contour. No unmagnetized, meandering effects are recognized, meaning a saturation of the transport process at the adiabatic regime. The drift, nevertheless, reveals inhomogeneities resembling the "walk-and-rest" statistics, manifest in the phases of "fast" and "slow" cross-field propagation. These signatures, already noticeable for larger injection velocity 5×10^{-4}, now entirely dominate the dynamics.

V. SUMMARY AND CONCLUSIONS

We have analyzed the dispersion of charged particles in a synthesized magnetic field configuration composed of a constant homogeneous background field and a multiscale perturbation component simulating the effect of turbulence on the test-particle dynamics. Already for such a simple magnetic field model, we observe complex microscopic behavior of the charge carriers, demonstrating chaotic alternation of periods of rest and active cross-field migration regimes reminiscent of Levy-walk statistics. The integral process looks like a competition between rests and walks governing the transport properties on the microscopic scales.

In absence of the background component, the cross-field transport is almost diffusive, showing linear growth of the mean-square particle displacement versus time. At the microscopic level, this regime profits from an intricate compromise between the time intervals the particles stay in traps and the periods they actively propagate through the medium. Such complex features are in contrast with the conventional Brownian random motion paradigm, often associated with diffusion. With increasing background field, the equilibrium between rests and walks – the two constituents of the motion – shifts toward longer rests, leading to a sublinear (subdiffusive) behavior of the particle dispersion. We emphasize that the walks are inherently present in the microscopic picture of the dynamics, though the contribution they bring to the dispersion may be suppressed by the effect of rests. Two distinct subdiffusive regimes have further been recognized, depending on the injection velocity v (i.e., on the particle Larmor radius, $\ell \sim vmc/aqB$).

In the numerical model, a suitable range for the velocity v is allocated – in dimensionless units – from 2×10^{-4} to 5×10^{-4}. For the larger values of $v \sim 5 \times 10^{-4}$ enabling moderate nonadiabaticity of the charge carriers, the cross-field transport is concentrated on percolating fractal arrays associated with the zero-set of the perturbation component, $\delta B(\mathbf{r}) = 0$. In two ambient dimensions, the percolation along the zero-set is critical, meaning a threshold at the level $B = B_0$. The value of the transport exponent as predicted by the percolation-based model equals $\mu \approx 0.80$. This result – deriving from the fundamental properties of universality of the percolation transition – is reproduced in the simulation, $\mu \approx 0.84 \pm 0.05$. A characteristic feature of the percolation regime is the presence of chaotic meandering motion in a thin layer enveloping the separatrix $B = B_0$, mixed with gyromotion and trapping.

As the velocity is turned to $v = 2 \times 10^{-4}$, the transport exponent drops to $\mu \approx 0.67 \pm 0.05$. This behavior is reminiscent of the static limit $\mu \approx 0.58$ of stochastic Hamiltonian systems with $1\frac{1}{2}$ degrees of freedom. The tendency toward Hamiltonian dynamics reflects the proposed decrease in v in the presence of the background field. Some deviation between the numerical estimate of $\mu \approx 0.67 \pm 0.05$ and the extreme of $\mu \approx 0.58$ may further be shown to be due to the excessive effect of the magnetic perturbation introduced in the simulation. This effect decays with increasing background field.

A main result of the analytical investigation – performed in parallel with the numerical study – is that the regime of Hamiltonian dynamics is separated from random walk processes on a percolative fractal geometry by a gap in the transport exponent, $\Delta\mu \approx 0.12$. In the numerical simulation, the gap appears in an uncertain behavior of the particle dispersion for some intermediate values of $2 \times 10^{-4} \lesssim v \lesssim 5 \times 10^{-4}$. Within this interval, the exponent μ fluctuates between Hamiltonian-like ($\approx 0.67 \pm 0.05$) and fractal random walk-like ($\approx 0.84 \pm 0.05$) dispersion. The uncertanities are generally bypassed as v gets sufficiently close to 2×10^{-4}.

As the Hamiltonian regime is approached, the meandering counterpart of the particle dynamics vanishes. In this limit, the cross-field transport is dominated by long-time particle rests near the points of occasionally small magnetic gradients. Posing slight nonadiabaticity readily calls for the meandering to come into play. The transport exponent μ then promptly returns to the fractal random walk-like dispersion. With increasing nonadiabaticity the asymptotic diffusive regime is recovered starting from longer integration times. This result incorporates the effect of the finite fractal correlation length, posed by the basic periodicity of the simulation box.

ACKNOWLEDGMENTS

It is a pleasure to thank our colleagues E. Lazzaro, M. Lontano, H. L. Pecseli, J. J. Rasmussen, K. Rypdal, P. Veltri, L. M. Zelenyi, and F. Zonca for illuminating and lively discussions, and P. Pommois for his help in the numerical work. One of the authors (A.V.M.) gratefully acknowledges the very warm hospitality at the University of Calabria, where this study was initiated. During his stay in Italy, A.V.M. was supported by the grants of Italian INFM and MURST, and by the Agenzia Spaziale Italiana, contract no. I/R122/01. In Russia, this study was sponcored by the Science Support Foundation, by the Foundation for Basic Research (project 03-02-16967), and by the "School-of-Science" Grant 1739.2003.2. Partial support was received from INTAS project 03-51-3738. In Italy, this work was granted by the Cofin 2002 (MIUR) and by the Center for High Performance Computing (HPCC) of the University of Calabria (Centro di Eccellenza MIUR). The final version of this paper was prepared at the University of Tromsø, where A.V.M. stayed on a grant from the Research Council of Norway.

---

[1] D. Tetreault, J. Geophys. Res. **97**, 8541 (1992); K. Rypdal, J.-V. Paulsen, Ø. E. Garcia, S. Ratynskaya, and V. Demidov, Nonlinear Proc. Geophys. **10**, 139 (2003).

[2] R. A. Treumann, Physica Scripta **59**, 19 (1999); ibid. **59**, 204 (1999); A. V. Milovanov and L. M. Zelenyi, Adv. Space Res. **30**, 2667 (2002).

[3] E. W. Montroll and M. F. Shlesinger, in *Studies in Statistical Mechanics*, edited by J. Lebowitz and E. W. Montroll (North-Holland, Amsterdam, 1984), Vol. 11, p. 1.

[4] J. Klafter, M. F. Shlesinger, and G. Zumofen, Phys. Today **49**, 33 (1996).

[5] G. Zimbardo, P. Veltri, G. Basile, and S. Principato, Phys. Plasmas **2**, 2653 (1995); P. Pommois, G. Zimbardo, and P. Veltri, Phys. Plasmas **5**, 1288 (1998).

[6] S. Denisov, J. Klafter, and M. Urbakh, Physica D **187**, 89 (2004).

[7] B. D. Hughes, E. W. Montroll, and M. F. Shlesinger, J. Stat. Phys. **28**, 111 (1982).

[8] H. Scher, M. F. Shlesinger, and J. T. Bendler, Phys. Today **44**, 26 (1991).

[9] B. B. Mandelbrot and J. W. Van Ness, SIAM Rev. **10**, 422 (1968).

[10] J. Feder, *Fractals* (Plenum, New York, 1988).

[11] J. Klafter, A. Blumen, and M. F. Shlesinger, Phys. Rev. A **35**, 3081 (1987).

[12] W. D. Luedtke and U. Landman, Phys. Rev. Lett. **82**, 3835 (1999).

[13] G. M. Zaslavsky, Chaos **5**, 653 (1995).

[14] I. M. Sokolov, J. Klafter, and A. Blumen, Phys. Today **55**, 48 (2002).

[15] M. F. Shlesinger, G. M. Zaslavsky, and J. Klafter, Nature (London) **363**, 31 (1993).

[16] R. Metzler and J. Klafter, Phys. Rep. **339**, 1 (2000).

[17] G. M. Zaslavsky, Phys. Rep. **371**, 461 (2002).

[18] Y. Gefen, A. Aharony, and S. Alexander, Phys. Rev. Lett. **50**, 77 (1983).

[19] G. M. Zaslavsky and R. Z. Sagdeev, *Introduction to Nonlinear Physics. From Oscillator to Turbulence and Chaos* (Nauka, Moscow, 1988).

[20] B. O'Shaughnessy and I. Procaccia, Phys. Rev. Lett. **54**, 455 (1985); Phys. Rev. A **32**, 3073 (1985).

[21] A. V. Milovanov and G. Zimbardo, Phys. Rev. E **62**, 250 (2000).

[22] L. M. Zelenyi and A. V. Milovanov, Physics-Uspekhi **47** (8), 749 (2004) [Original Russian text: Uspekhi Fizicheskikh Nauk **174** (8), 809 (2004)].

[23] T. Nakayama, K. Yakubo, and R. L. Orbach, Rev. Mod. Phys. **66**, 381 (1994).

[24] J.-P. Bouchaud and A. Georges, Phys. Rep. **195**, 12 (1990).

[25] J. Viecelli, Phys. Fluids A **5**, 2484 (1993); T. Solomon, E. Weeks, and H. Swinney, Phys. Rev. Lett. **71**, 3975 (1993); D. Elhmaidi, A. Provenzale, and A. Babiano, J. Fluid Mech. **257**, 553 (1993); A. Provenzale, Annu. Rev. Fluid Mech. **31**, 55 (1999).

[26] A. H. Nielsen, H. L. Pecseli, and J. J. Rasmussen, Phys. Plasmas **3**, 1530 (1996).

[27] V. Naulin, A. H. Nielsen, and J. J. Rasmussen, Phys. Plasmas **6**, 4575 (1999).

[28] X. Leoncini and G. M. Zaslavsky, Phys. Rev. E **65**, 046216 (2002).

[29] S. Caracciolo, M. S. Causo, P. Grassberger, and A. Pelissetto, J. Phys. A **32**, 2931 (1999).

[30] A. V. Milovanov and J. J. Rasmussen, Phys. Rev. B **64**, 212203 (2001).

[31] G. Zimbardo, Commun. in Nonlinear Science and Numerical Simulation **8**, 443 (2003).

[32] G. M. Zaslavsky, M. Edelman, H. Weitzner, B. Carreras, G. McKee, *et al.*, Phys. Plasmas **7**, 3691 (2000).

[33] B. A. Carreras, B. van Milligen, M. A. Pedrosa, R. Balbin, C. Hidalgo, *et al.*, Phys. Rev. Lett. **80**, 4438 (1998); B. A. Carreras, B. van Milligen, C. Hidalgo, R. Balbin, E. Sanchez, *et al.*, Phys. Rev. Lett. **83**, 3653 (1999); B. A. Carreras, V. E. Lynch, and B. LaBombard, Phys. Plasmas **8**, 3702 (2001).

[34] A. V. Milovanov and L. M. Zelenyi, Phys. Fluids B **5**, 2609 (1993).

[35] A. V. Milovanov and L. M. Zelenyi, in *Physics of the*

Magnetopause, Geophysical Monograph No 90, edited by P. Song, B. U. O. Sonnerup, and M. F. Thomsen (American Geophysical Union, Washington, DC, 1995), p. 357.
[36] A. Greco, A. L. Taktakishvili, G. Zimbardo, P. Veltri, G. Cimino, *et al.*, J. Geophys. Res. **108**, 1395 (2003).
[37] A. V. Milovanov, L. M. Zelenyi, and G. Zimbardo, J. Geophys. Res. **101**, 19 903 (1996); G. Zimbardo, A. Greco, and P. Veltri, Phys. Plasmas **7**, 1071 (2000).
[38] A. V. Milovanov, L. M. Zelenyi, G. Zimbardo, and P. Veltri, J. Geophys. Res. **106**, 6291 (2001).
[39] C. Chu, M.-S. Chu, and T. Ohkawa, Phys. Rev. Lett. **41**, 653 (1978).
[40] J. B. Taylor and B. McNamara, Phys. Fluids **14**, 1492 (1971).
[41] V. L. Ginzburg and A. A. Ruhadze, in *Handbuch der Physik*, edited by S. Flugge (Springer, Berlin, 1972), Vol. XLIX, p. 459.
[42] M. Hoshino, A. Nishida, T. Yamamoto, and S. Kokubun, Geophys. Res. Lett. **21**, 2935 (1994); M. Hoshino, T. Mukai, A. Nishida, Y. Saito, T. Yamamoto, *et al.*, J. Geomag. Geoelectr. **48**, 515 (1996).
[43] M. B. Isichenko, Rev. Mod. Phys. **64**, 961 (1992).
[44] V. Naulin, Ø. E. Garcia, A. H. Nielsen, and J. J. Rasmussen, Phys. Lett. A **321**, 355 (2004).
[45] N. A. Krall and A. W. Trivelpiece, *Principles of Plasma Physics* (McGraw-Hill, New York, 1973).
[46] A. Brissaud and U. Frisch, J. Math. Math. **15**, 524 (1974).
[47] A. V. Milovanov, Phys. Rev. E **63**, 047301 (2001).
[48] J.-D. Reuss and J. H. Misguich, Phys. Rev. E **54**, 1857 (1996).
[49] D. Stauffer and A. Aharony, *Introduction to Percolation Theory* (Taylor & Francis, London, 1992).
[50] S. Alexander, and R. L. Orbach, J. Phys. (France) Lett. **43**, L625 (1982).
[51] A. V. Milovanov, Phys. Rev. E **56**, 2437 (1997).
[52] A. V. Milovanov and J. J. Rasmussen, Phys. Rev. B **66**, 134505 (2002).
[53] M. Schroeder, *Fractals, Chaos, Power Laws* (W. H. Freeman, New York, 1991).
[54] V. G. Boltyanskyi and V. A. Efremovich, *Descriptive Topology* (Nauka, Moscow, 1983).

FIG. 1. A zero cut $\delta B(\mathbf{r}) = 0$ of the fractional Brownian surface in Eqs. (4) and (5), corresponding to the exponent of the Fourier energy density spectrum $\alpha = 3/2$. Owing to the sign parity $\delta B(\mathbf{r}) \leftrightarrow -\delta B(\mathbf{r})$, the cut $\delta B(\mathbf{r}) = 0$ contains a percolating isoenergetic contour enabling charged-particle transport across the field already in the limit of adiabatic dynamics.

FIG. 2. A track of a test-particle injected in close vicinity of the zero-set $\delta B(\mathbf{r}) = 0$ and propagating to longest distances present. The background component is zero everywhere, $B_0 = 0$, corresponding to the infinite value of the perturbation parameter, $b = \infty$. The injection velocity equals $v = 5 \times 10^{-4}$. Dimensionless units.

FIG. 3. A typical test-particle trajectory underlying the "strange diffusion." All the same injection and magnetic realization parameters as in Fig. 2. Dimensionless units.

FIG. 4. The particle dispersion as a function of time for the finite perturbation parameter, $b \sim 2$. The injection velocity set to $v = 5 \times 10^{-4}$. The integration covers time scales up to 3×10^6. Both runs with (dashed line) and without (solid line) the filter are shown. In absence of the filter, the particles are injected everywhere at random. The filter discards the particles found "too far" from the percolation level.

FIG. 5. A track of a particle faced to random walk process on a percolative fractal geometry. Note the characteristic meandering motion mixed with inhomogeneous drift-like migration along the separatrix.

FIG. 6. The particle dispersion versus time for two different values of the injection velocity, $v = 5 \times 10^{-4}$ (solid line) and $v = 2 \times 10^{-4}$ (dashed line). Finite perturbation parameter, $b \sim 2$. The integration is performed up to 1×10^7.

FIG. 7. A track of a nearly magnetized particle migrating along the percolating isoenergetic contour. In contrast to the trajectory in Fig. 5, no meandering-like motion is present. Dimensionless units.

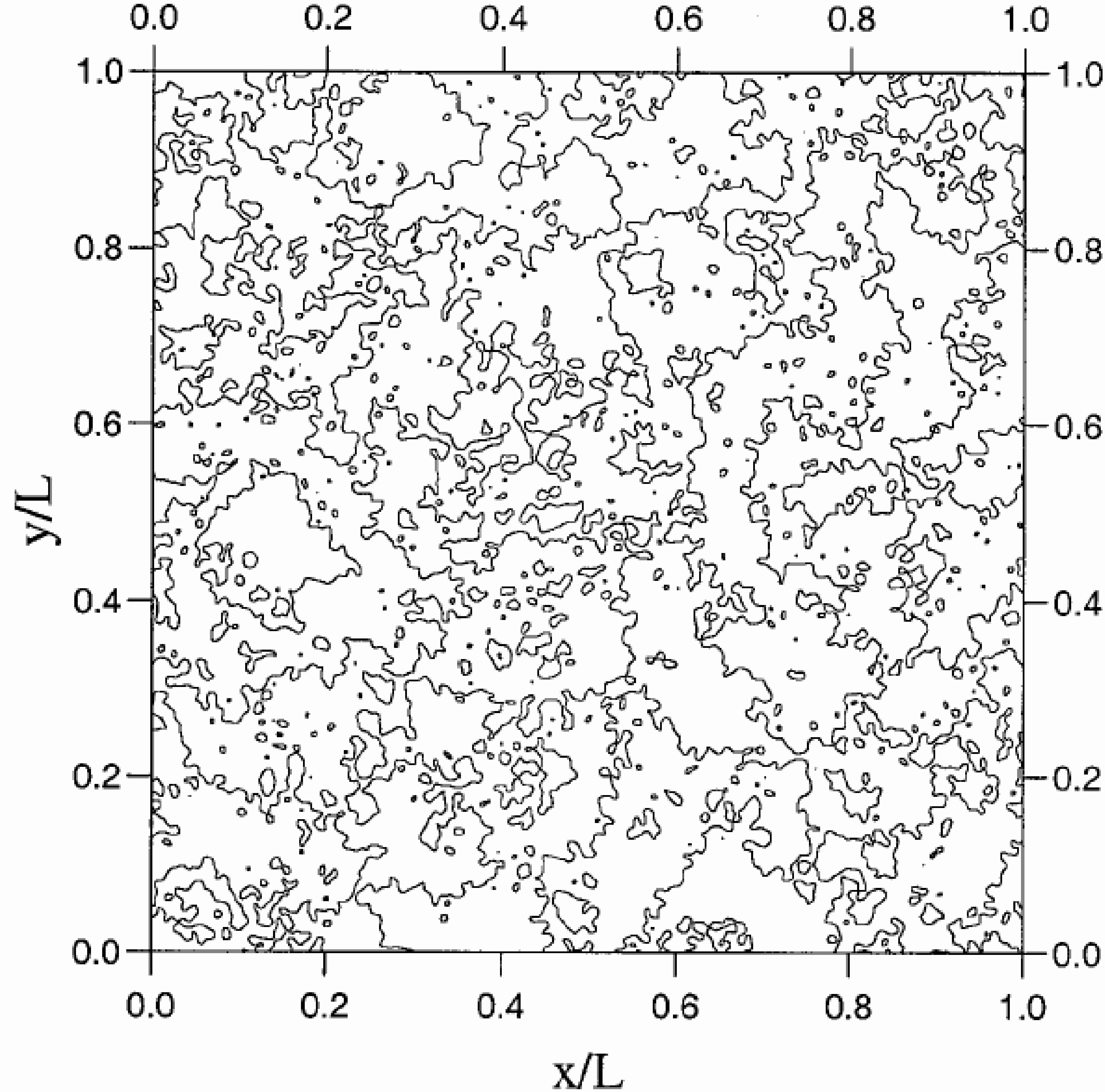

0.0
0.2
0.4
0.6
0.8
1.0
y/L
x/L

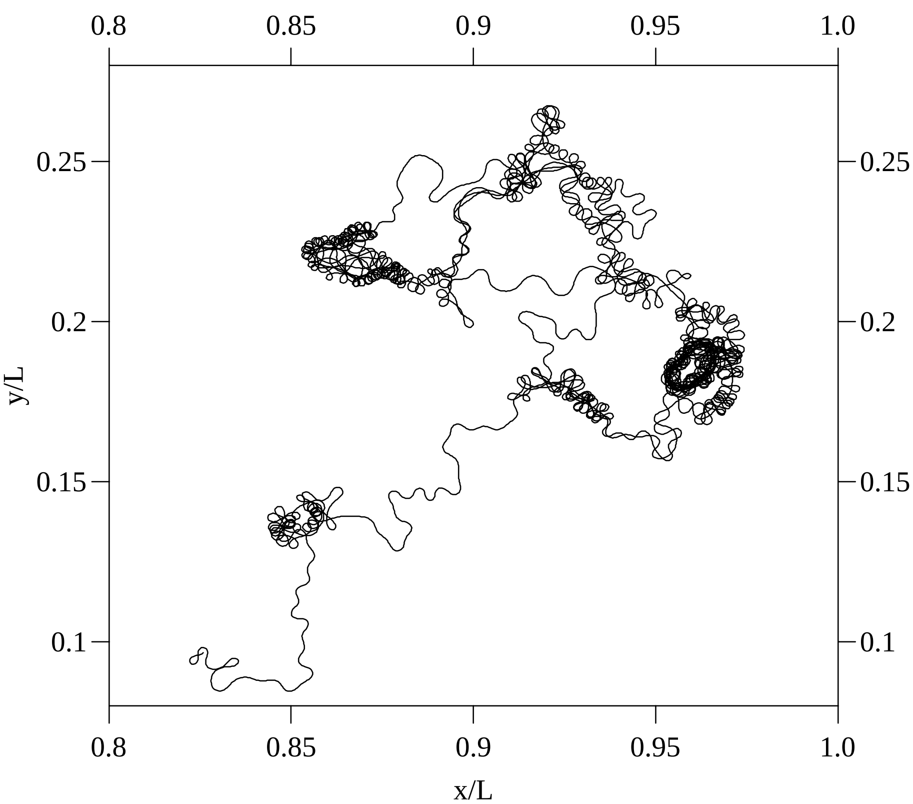
0.8
0.85
0.9
0.95
1.0
0.25
0.2
0.15
0.1
y/L
x/L

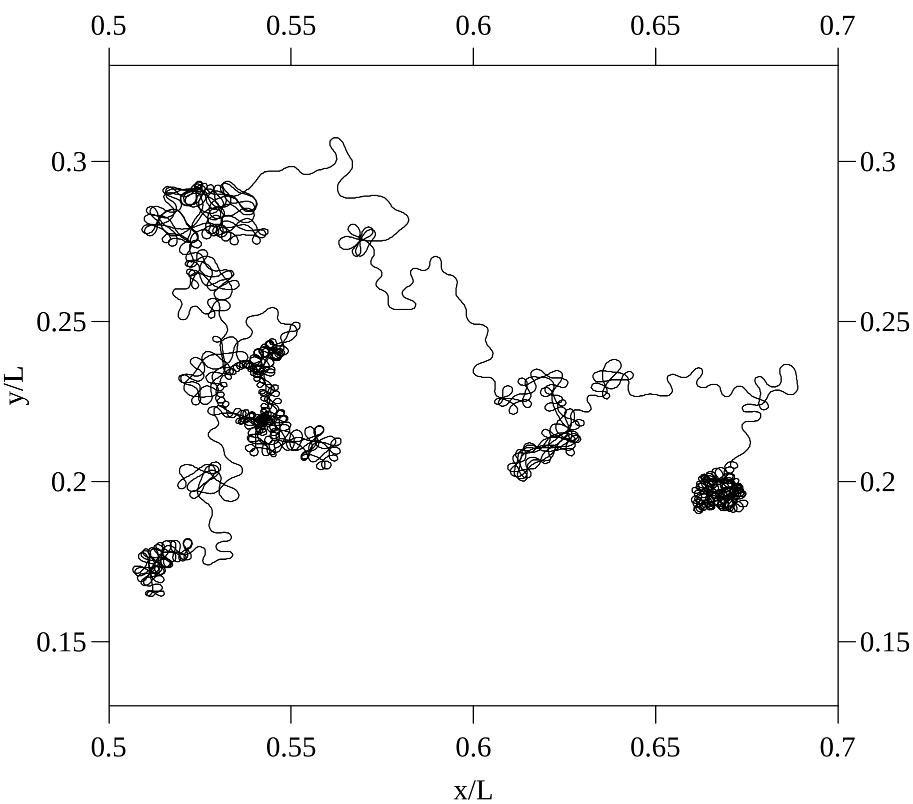
0.5
0.55
0.6
0.65
0.7
0.3
0.25
0.2
0.15
y/L
x/L

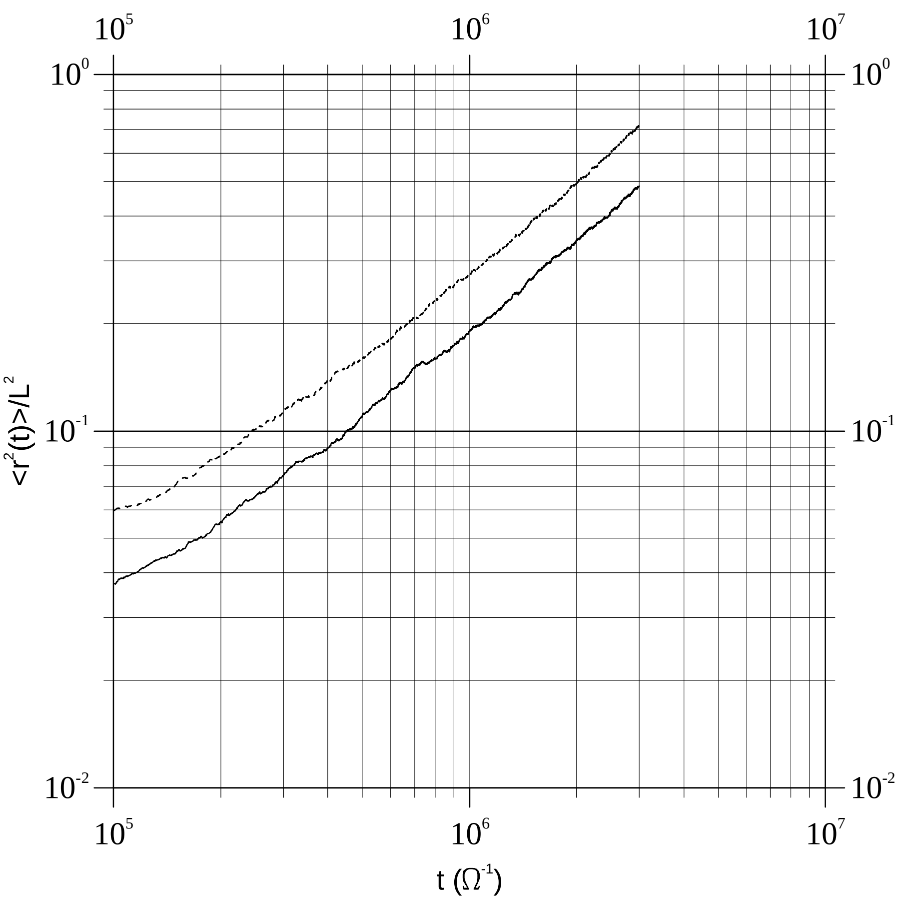

10^5
10^6
10^7
10^0
10^{-1}
10^{-2}
$<r^2(t)>/L^2$
t (Ω^{-1})

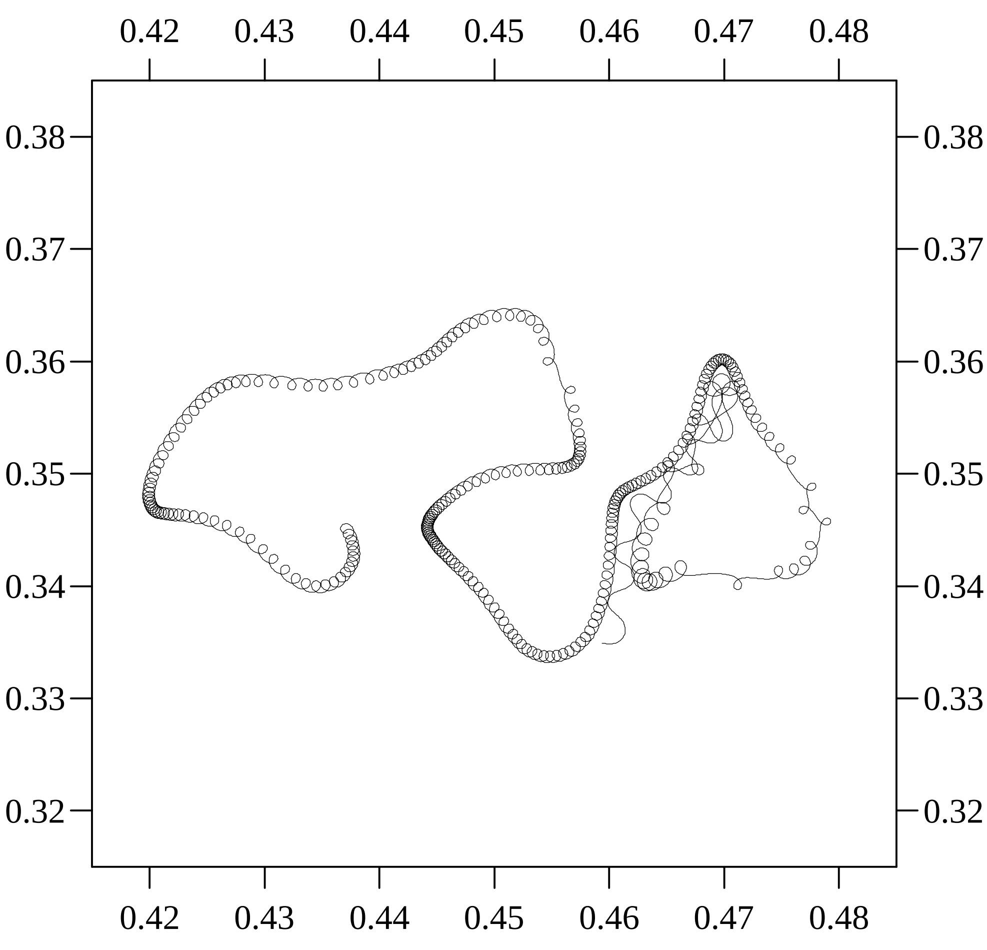
0.42
0.43
0.44
0.45
0.46
0.47
0.48
0.38
0.37
0.36
0.35
0.34
0.33
0.32

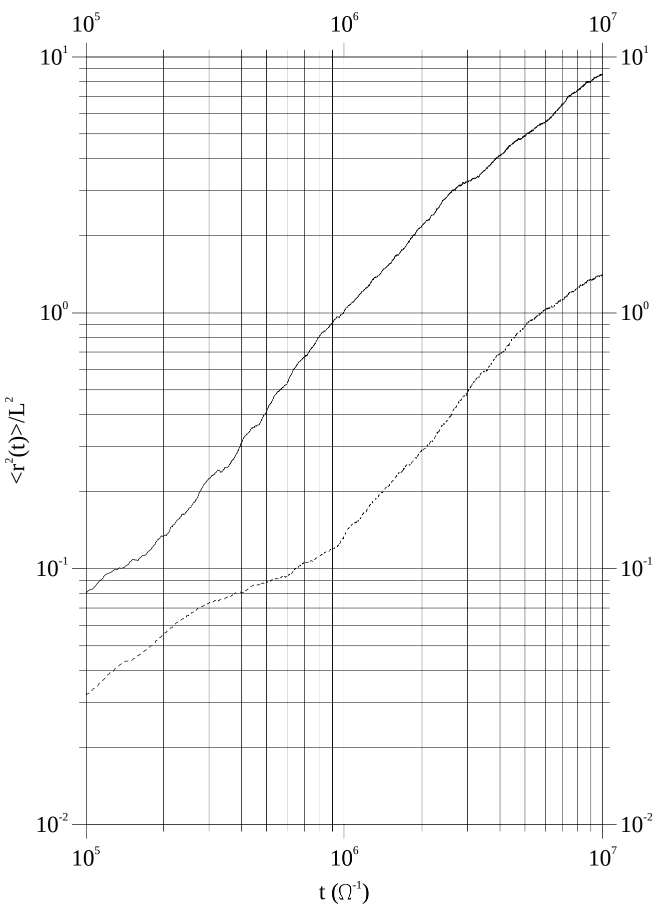

10^5
10^6
10^7
10^1
10^0
10^-1
10^-2
<r^2(t)>/L^2
t (Ω^-1)

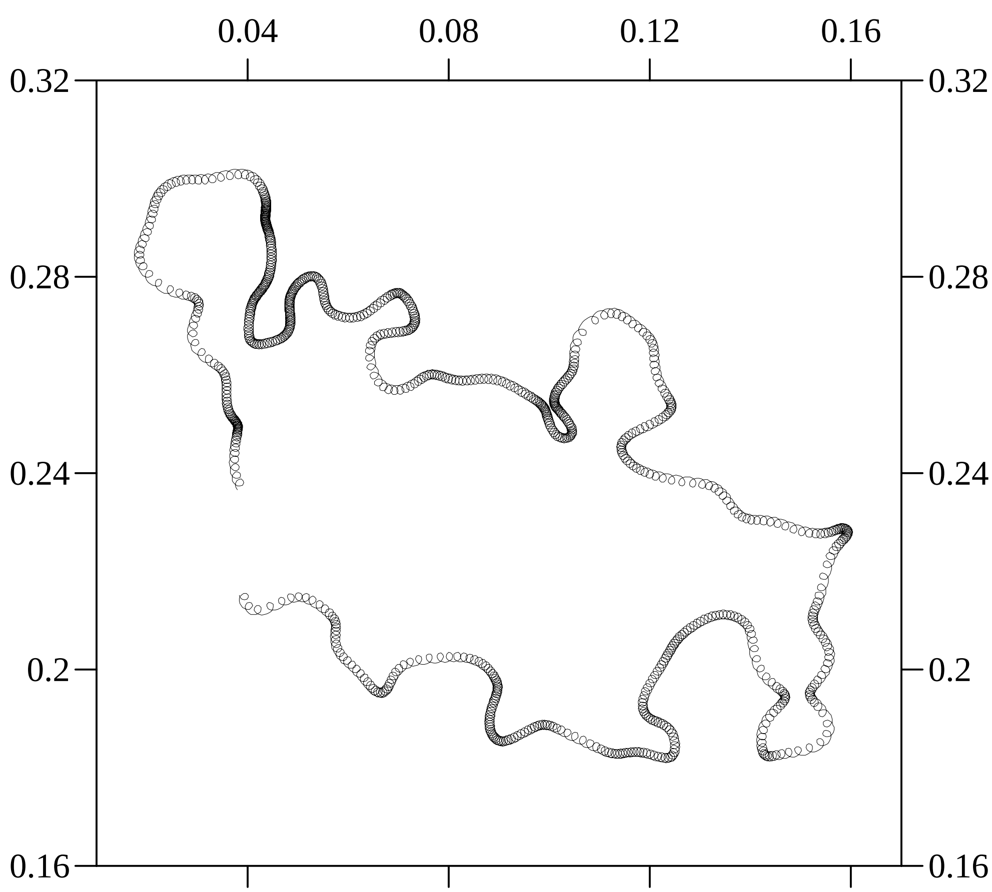
0.04
0.08
0.12
0.16
0.32
0.28
0.24
0.2
0.16